Electrochemical dating of archaeological gold based on refined peak current determinations and Tafel analysis

Antonio Doménech-Carbó[a], Fritz Scholz[b], Michael Brauns[c], SianTiley-Nel[d], Arturo Oliver[e], Gustavo Aguilella[f], Noemí Montoya[a], María Teresa Doménech-Carbó[g]

[a] Department of Analytical Chemistry, University of Valencia, Dr. Moliner, 50, 46100, Burjassot (Valencia), Spain
[b] Universität Greifswald, Institut für Biochemie, Felix-Hausdorff Straße 4, 17487, Greifswald, Germany
[c] Curt-Engelhorn-Zentrum Archäometrie gGmbH, D6,3 (OG 3), 68159, Mannheim, Germany
[d] Faculty of Humanities, Department of Historical and Heritage Studies, University of Pretoria & University of Pretoria Museums, Old Arts Building University of Pretoria, Private Bag X20, Hatfield, 0028, South Africa
[e] Museu de Belles Arts de Castelló, Avenida Hermanos Bou, 28, 12003, Castellón de la Plana, Spain
[f] Servicio de Investigaciones Arqueológicas y Prehistóricas, Diputación de Castellón Avda, Hnos Bou 28 (edificio Museu), 12003, Castellón, Spain
[g] Institut de Restauració del Patrimoni, Universitat Politècnica de València, Camí de Vera 14, 46022, València, Spain

*Corresponding author. antonio.domenech@uv.es

Highlights

- Electrochemical dating of archaeological gold samples is based on the voltammetry of immobilized particles.
- Samples from the Mapungubwe Gold Collection (1200–1290 CE) and Santa Llúcia archaeological site (600-550 BCE) were studied.
- Peak potentials and peak currents for gold oxidation in 0.10 M HCl are used.

Abstract

This report proposes a refined method to date archaeological gold samples based on the Tafel analysis of the ascending part of voltammetric curves corresponding to the oxidation of surface flakes of gold in contact with hydrochloric acid aqueous electrolyte. This allows estimating the equilibrium potential of gold oxidation correcting for irreversibility effects. This equilibrium potential can be correlated with the coverage of adsorbed oxygen species and hence the estimated age of the gold samples. A satisfactory potential/time calibration graph was constructed from a set of archaeological samples including two sets of samples from the Mapungubwe Gold Collection, South Africa (1200–1290 CE) and Santa Llúcia, Alcalà de Xivert in Spain (dated back 600-550 BCE) sites. The dated samples come not only from different continents, but their ages also cover more than 3000 years.

Graphical abstract

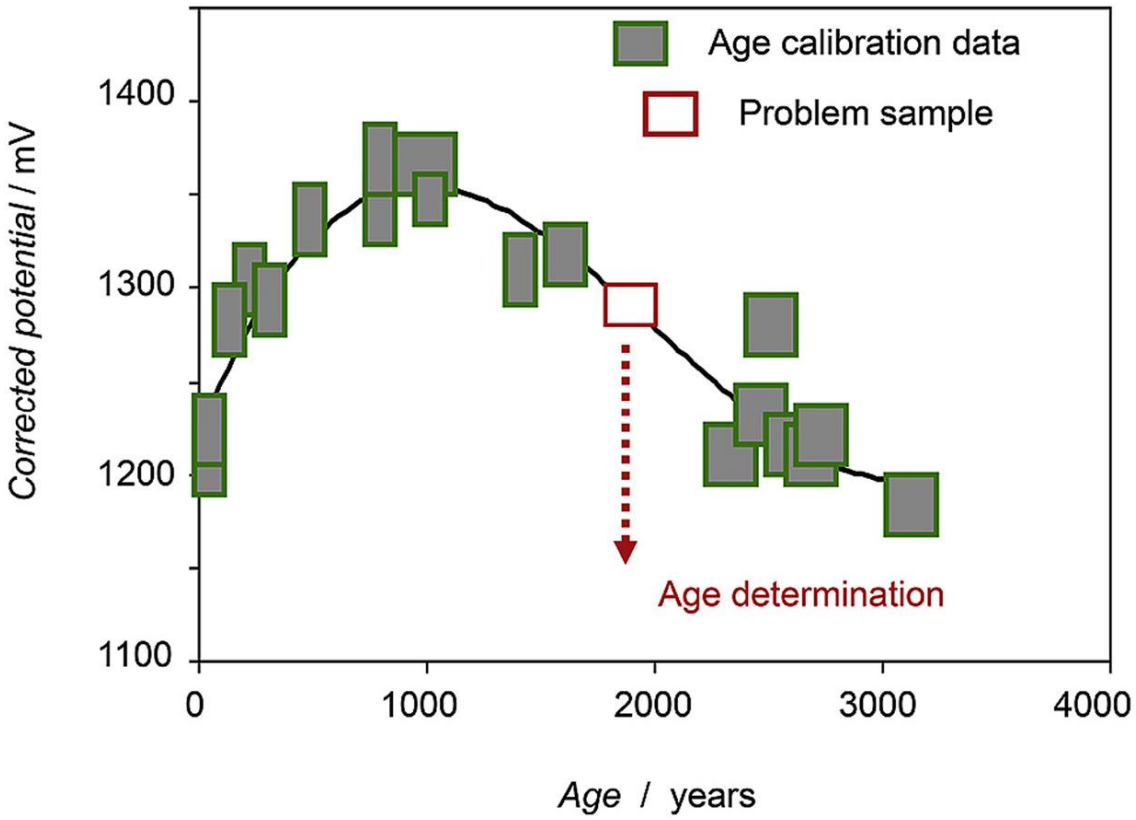

Keywords: Gold; Dating; Tafel; Archaeology; Electrochemistry

1. Introduction

Dating of ancient metals is an important analytical aim in archaeology, historical and conservation science, arts and other related disciplines. This is a real challenge due to the unavailability of the majority of techniques (e.g., radiocarbon, uranium decay, thermoluminescence, obsidian hydration) to date metals [1,2]. Recently, methods for dating lead using the Meissner superconducting effect [3], and gold based on He, U, and Th analysis [4,5] have been described. However, these methods suffer from the need of rather large amounts of samples (some hundred milligrams), thus requiring an invasive (destructive) sampling procedure. Here a minimally invasive sampling and electrochemical analysis method is proposed, which requires just a few nanograms.

Aimed to complement the existing techniques for metal dating, the application of solid state voltammetry for dating lead [6], copper/bronze [7], and gold [8] samples has been previously described. These methods exploit the high sensitivity of the voltammetry of immobilized particles (VIMP) [[9], [10], [11]], a solid state electrochemistry technique that provides sensitive responses restricting the sampling to only a few nanograms collected on the metal surface by means of graphite leads [12,13]. Based on this methodology, widely used in the analysis of archaeological, historic and art objects in the science of conservation and restoration field [14,15], and primarily proposed as applicable to date ceramic materials [16],

chronological information on lead-bronze statuary [17] and coinage [18], gold altarpieces [19] and embroidery [20] has been made available.

As all other 'chemical' dating methods, e.g., the obsidian hydration and amino acid racemization [21,22], the application of these voltammetric methodologies requires the assumptions that the chemical conditions were rather constant over time. A second aspect to be accounted for is that the composition of the corrosion layers of metals depends in general on the depth with a concomitant effect on the voltammetric responses [23].

In this context, electrochemical dating of archaeological gold is of particular interest because its voltammetric behaviour is rather well known [[24], [25], [26], [27], [28], [29], [30], [31], [32], [33], [34], [35], [36], [37], [38], [39]], and, due to its noble character, the aging of this metal is much less sensitive to the 'local' physico-chemical conditions and their possible fluctuations over the entire time span to be dated. However, the electrochemical response of archaeological gold artefacts can be sensitive to the composition of the base metal (silver content in particular) and the manufacturing process. Archaeological gold alloys (gold-silver, gold-copper, gold-copper-silver) deteriorate in different ways which enhances the difficulties of preservation and their dating. As a result, previous data using a set of gold coins and different archaeological objects, provided a calibration graph with relatively high dispersion [8]. Here, an improved electrochemical methodology for archaeological gold dating is reported based on: i) refined peak current measurements, and ii) the Tafel analysis of the voltammetric curves.

In the current work, a series of samples from the Museum of Fine Arts of Castelló (Spain), Museum of Mannheim (Germany), and University of Pretoria Museums (South Africa) were studied. These include two sets of particularly relevant samples: the Mapungubwe Gold Collection (Republic of South Africa), dated back to 1200–1290 CE [40,41], and the collection from the Santa Llúcia, Alcalà de Xivert (Spain), dating back to 600-550 BCE [42]. These correspond to objects recovered from burials having in principle the same age thus prompting the study of the influence of possible differences in manufacturing and/or composition of the objects in the dating.

It is pertinent to underline that, by reasons of conservation, the sampling (consisting of pressing a graphite electrode onto the surface of the objects, as previously applied [[14], [15], [16], [17], [18], [19], [20]]) was limited to three spots in each archaeological object. As a result, we obtained three replicate voltammetric measurements for each sample/object. The sampling was carried out in the museums by the researchers of the respective institutions and the electrodes were mailed to the University of Valencia where the voltammetric measurements were performed. Due to the limited number of accessible samples, we used the three-step voltammetric protocol in 0.10 M HCl solution already described [8] in order to maximize the analytical signals able to be processed. In order to test the suitability of the proposed dating methodology, one of the samples, one wire ring (MA01, "im Grafenwald" Hermeskeil) from the Rheinische Landesmuseum Trier was taken as a problem sample. This sample is representative of a frequent problem in archaeology: the disposal of samples coming from non-professional excavations or corresponding to sites with ill-defined stratigraphy. As judged by its archaeological context, the estimated age of sample MA01 was 30–150 BCE. However, as far as the relation of the object with the context was not entirely known, there was uncertainty about its age. Accordingly, this sample was treated as a problem sample of unknown age by the electrochemistry research team.

The detailed description of the samples is provided in Table 1. Voltammetric data are combined with Raman spectroscopy and focusing ion beam-field emission scanning electron microscope (FIB-FESEM) and high resolution field emission scanning electron microscopy (HRFESM-EDX). By the aforementioned reasons of conservation, these techniques were applied only to contemporary gold objects taken as a reference.

Table 1. Characteristics of the gold samples in this study. MA: Mannheim Museum; SA: Mapungubwe Collection, University of Pretoria Museums (South Africa), Sample MA01 corresponds to a ring from the Rheinische Landesmuseum Trier; SLL: Santa Llúcia, Alcalà de Xivert, Museu de Belles Arts de Castelló; PC: private collections.

Sample	Description/Catalogue number	Date
SL01	Ingot, SLL18-1 h	575 BCE
SL02	Ingot, SLl18-1a	575 BCE
SL03	Ingot, SLl18-1c	575 BCE
SL04	Ingot, SLl18-1e	575 BCE
SL05	Ingot, SLl18-1 g	575 BCE
MU01	Gold foil, Mapungubwe Hill grave area (M1 A620)	1200-1290 CE
MU02	Gold foil, Mapungubwe Hill grave area (M1 A620)	1200-1290 CE
MU03	Gold foil, Mapungubwe Hill grave area (M1 A620)	1200-1290 CE
MU04	Gold foil, Mapungubwe Hill grave area (M1 A620)	1200-1290 CE
MU05	Gold foil, Mapungubwe Hill grave area (M1 A620)	1200-1290 CE
MU06	Gold helix, Mapungubwe Hill grave area (M7 A623)	1200-1290 CE
MA01	Ring “im Grafenwald" Hermeskeil, WP129	
MA02	Lamina, MA184402	1600 BCE
MA03	Lamina, MA184414	1300-1400 BCE
MA04	Lamina, MA184428	1300-1400 BCE
MA05	Torq (Lydia-a)	650 BCE
MA06	Bullets added to torq (Lydia-b)	modern
MA07	Three bullets (‘Pilonquitos’)	900-1300 BCE
MA08	Figurine, MA446	modern
MA09	Torq from Chatonnaye, MA458	Ha D2/3 (600–500/480 BCE)
MA10	Foil, MA510	Ha D3 (550–480/500 BCE)
MA11	Foil, MA512	Ha D3 (550–480/500 BCE)
Z01	Ring^{PC}	1960 CE
Z02	Medal^{PC}	1902 CE
Z03	Ring^{PC}	1988 CE

2. Experimental details

2.1. Samples

Samples were taken from different gold objects from private collections (Z01-Z03), the Mapungubwe Gold Collection (MU01-MU06, Pretoria, South Africa), dated back to 1200–1290 CE [40,41], the collection from the Santa Llúcia (SL01 to SL05) at the Museum of Fine Arts of Castelló (Spain) and the Museum of Mannheim (MA01 to MA11). The samples included one recognized forgery (MA08) of undetermined 'modern' age, and one wire ring (MA01, "im Grafenwald" Hermeskeil) from the Rheinische Landesmuseum Trier that was tentatively dated back to 30-150 BCE. This sample was considered as a problem sample and all its study was performed without knowledge of its real age. The sampling was performed *in situ* on uncleaned (or smoothly cleaned with a brush) surfaces under controlled measures in a museum environment and the graphite lead bars were submitted for analyses.

2.2. Instrumentation and methods

Voltammetric experiments were performed at 298 ± 1 K in a three-electrode cell using a CH I660 potentiostat (Cambria Scientific, Llwynhendy, Llanelli UK) with a graphite working electrode, to the surface of which flakes of the gold surface have been transferred, a platinum wire auxiliary electrode, and an Ag/AgCl (3 M NaCl) reference electrode. 0.10 M HCl aqueous solution was used as a supporting electrolyte. To test the possibility of in-field measurements using available portable equipments, deaeration was optionally performed by bubbling Ar during 10–15 min prior to electrochemical runs. Sampling was performed *in situ* by lightly pressing graphite bars of diameter 2 mm (Faber-Castell, HS pencil leads) over plain surfaces of the archaeological samples in a controlled manner thus avoiding surface damage or appreciable abrasion. The resultant graphite mark is wiped off with ethanol or distilled water and the sampling spot remained visually unaffected on the gold surface. Sampling was conducted on both ends of the graphite bar permitting the duplication of measurements, the graphite bars were placed in Eppendorf vials for sending for analysis.

Raman spectra of samples Z02 and Z03 were obtained by means of XPlora Horiba MTB model using a 532 nm laser for excitation and keeping the samples in backscattering geometry at room temperature. A 100 confocal microscope objective was used to focus the excitation laser on the sample and to collect the scattered light to the spectrometer with exposure times between 5 and 20 s, 10–50 acquisitions, and laser power varying between 30 and 90 mW, respectively. Data acquisition was carried out with the LabSpec 6 Spectroscopy Suite from Horiba MTB. For Raman depth measurements, samples were mounted on an *x,y* motorized stage, with *z*-displacement controlled with a piezo-transducer on the objective. The confocal pinhole diameter was 20.0 cm, and the slit width was 10.0 cm.

The surface analysis runs to characterise the micromorphology and variations in the elemental composition in the surface and sub-surface of samples Z02 and Z03 was carried out by performing trenches using a field emission scanning electron microscope coupled to a focused ion beam Zeiss (Orsay Physics Kleindiek Oxford Instruments), model Auriga compact equipment. The operating conditions were: voltage, 30 kV and current intensity, 500 μA and 20 nA in FIB to generate the focused beam of Ga ions. The Ga beam impacts perpendicularly on the plane of the vertical wall of the trench by tilting the stage 54° where the object is placed. A voltage of 2 kV was used in FESEM to acquire electron images. For protecting the surface of the gold object during the application of the Ga beam the area where

the trench was performed was previously coated with a Pt layer with a thickness of 300 nm in an area of (8 × 10) μm.

The energy dispersive X-ray microanalysis was performed in trenches with a high resolution field emission scanning electron microscope (HRFESM-EDX) Zeiss (Orsay Physics Kleindiek Oxford Instruments) model GeminiSEM 500 with an Oxford-Instrument X-ray microanalysis, which was controlled by the Aztec software. A voltage of 5 kV and a working distance of 6–7 mm were applied. The ZAF method was followed to correct the interelemental effects in the semiquantitative microanalysis. A counting time of 100 s was used. The secondary electron images and X-ray spectra were obtained in cross-sections. The latter were acquired in the spot mode.

3. Results and discussion

3.1. Voltammetric pattern

Voltammetric data were taking following the three-step protocol previously described [8] consisting in the successive recording of the anodic-cathodic-anodic linear sweep voltammograms (LSVs) at sample-modified graphite electrodes immersed into 0.10 M HCl air-saturated aqueous solution. This sequence is illustrated in Fig. S1 (Supplementary information) for sample SL01. The voltammograms show common features for all studied samples (see Supplementary information, Fig. S2), without large differences between archaeological and 'modern' samples Z01-Z03 (see Fig. 4 and Fig. S3 in Supplementary information). The typical response is illustrated in Fig. 1 for the Mapungubwe sample MU01 (a) and the modern sample Z03 (b): In the initial positive-going potential scan, a weak stripping signal appears at 0.03 V vs. Ag/AgCl (A_{Ag} (1)) preceding a broad peak at 0.98 V (A_{Au} (1)) which precedes the prominent rising current at potentials above 1.25 V, corresponding to the oxygen evolution reaction (OER). No significant differences in the voltammetric response were obtained between air-saturated and deoxygenated solutions.

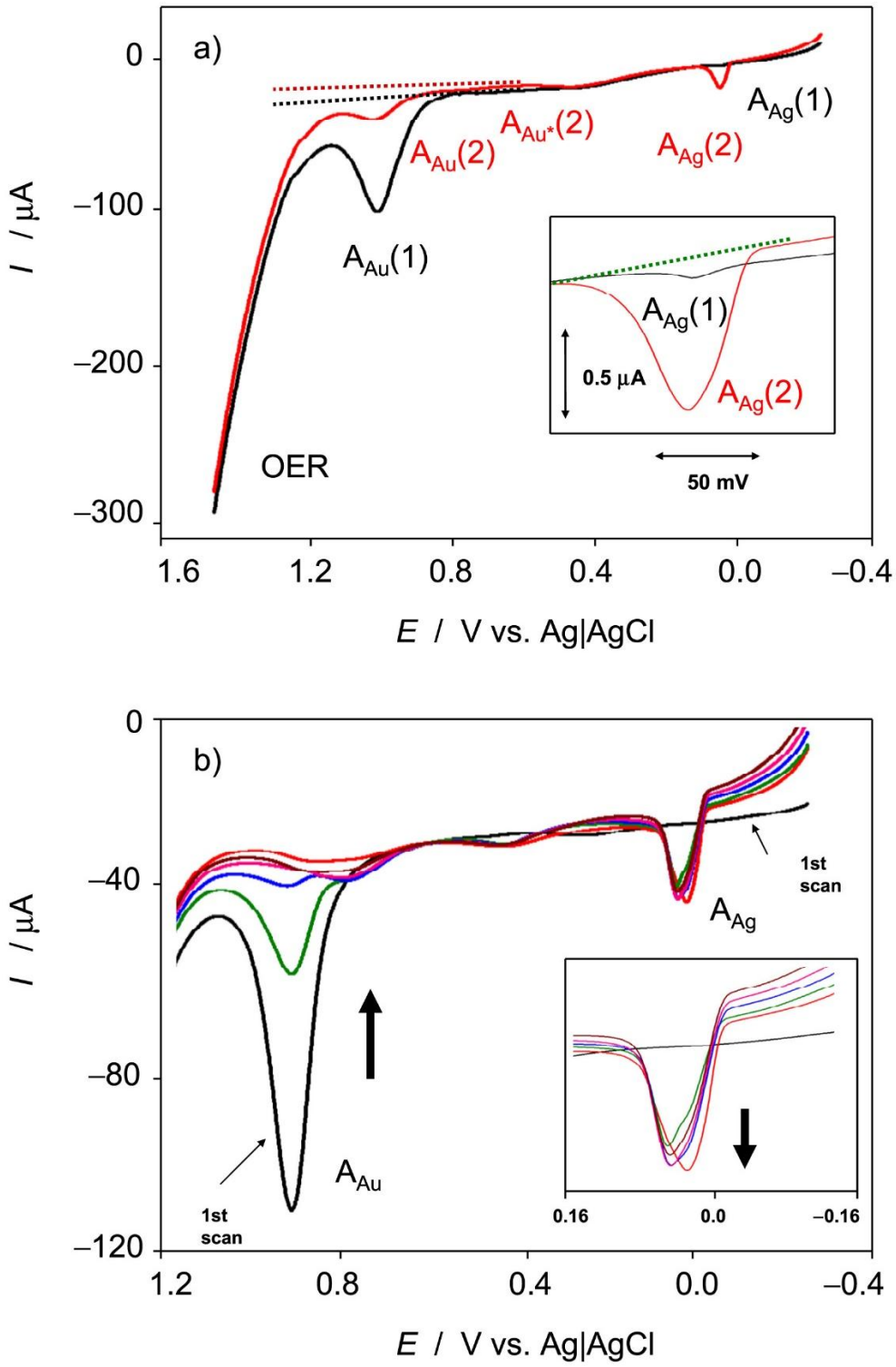

Fig. 1. LSV of gold samples attached to graphite electrode in contact with air-saturated 0.10 M HCl. a) First (black line) and second (red line) anodic LSVs of the Mapungubwe sample MU01. b) Successive anodic scans on sample Z03. The insets show the detail of the region of potentials where the Ag stripping occurs. The dotted lines are the base lines used for current measurements. Potential scan rate 50 mV s^{-1}.

Due to the high chloride concentration in the electrolyte, and based on blank experiments at silver electrodes, the signal A_{Ag} (1) can be attributed to the oxidation of Ag to AgCl, the

inverse process determining the appearance of the peak C_{Ag} in cathodic scans (see Fig. S1 in Supplementary information). In turn, the peak A_{Au} (1) corresponds to the oxidation of Au. In the presence of noncomplexing electrolytes this process yields a gold oxide monolayer [25,26,37,38] but in concentrated chloride media the oxidation leads to Au(III)-chloride complexes [24,38]. For simplicity, this can be represented as follows:

$$Au_{\,solid} + xCl^-_{\,aq} \rightarrow AuCl_x^{(x-3)-}_{\,aq} + 3e^- \qquad (1)$$

This electrochemical behaviour is reflected in secondary electron images of gold plates shown in Fig. 2 corresponding to sample Z02 (a gold medal manufactured in 1902) transferred onto a graphite bar in contact with 0.10 M HCl before (Fig. 2a) and after (Fig. 2b) application of a potential input of +1.25 V for 5 min. Voltammetric data on Z01-Z03 samples at potential scan rates between 5 and 500 mV s^{-1} in HCl solutions of concentrations between 0.01 and 1.0 M denoted that the repeatability in replicate experiments slightly increases on increasing scan rate while the signal-to-background ratio for peak A_{Au} (1) increases upon lowering the scan rate while the rate of Au dissolution increases with HCl concentration. Accordingly, the potential scan rate of 50 mV s^{-1} and 0.10 M HCl were selected to promote a significant but partial oxidative dissolution of gold (Fig. 2a,b) and a compromise between peak resolution and repeatability.

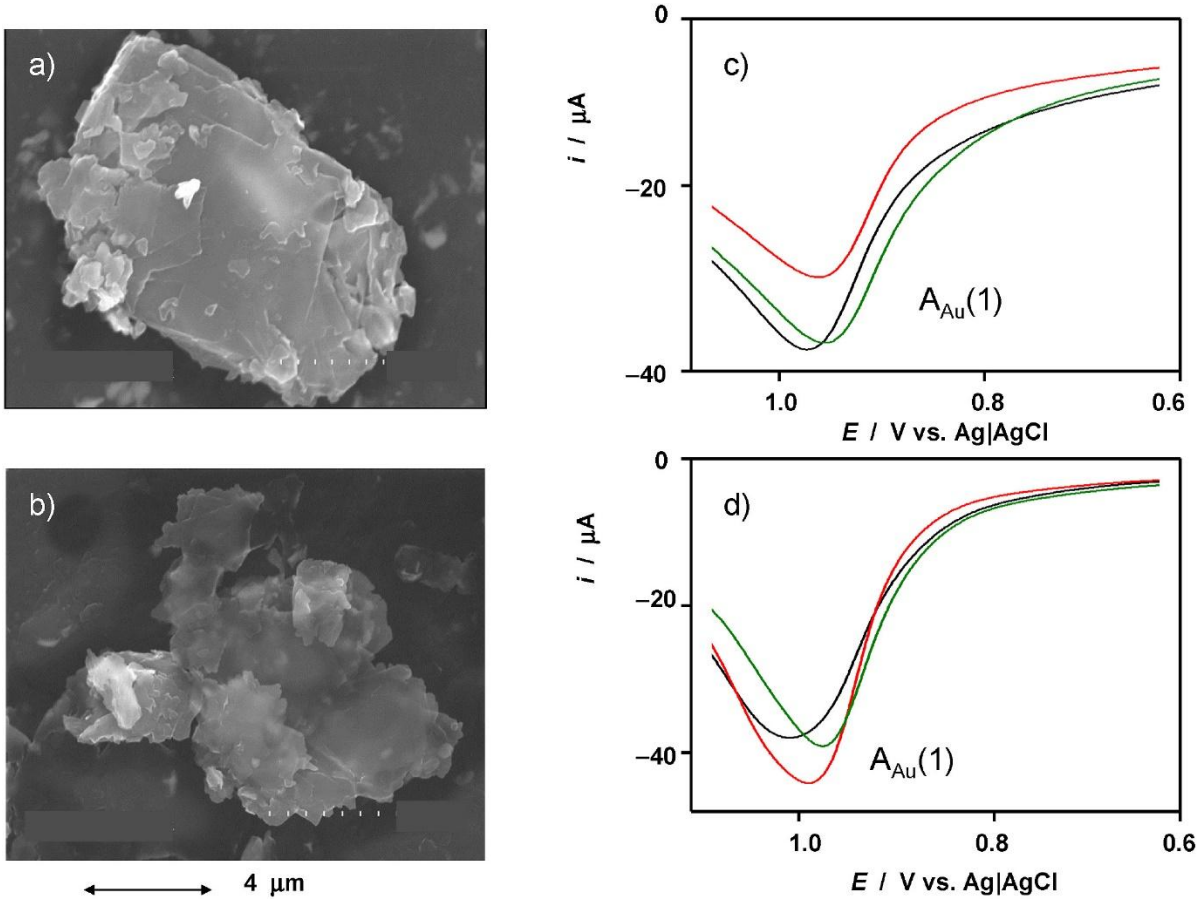

Fig. 2. a,b) Secondary electron images of gold plates from a medal fabricated in 1902 (sample Z02) abrasively transferred onto a graphite bar in contact with 0.10 M HCl aqueous solution: c) before and d) after application of a potential step of +1.25 V for 5 min. c,d) Detail of the signal A_{Au} (1) recorded in the first anodic LSVs (three replicate experiments) of samples c) SL03 and d) SL05 attached to graphite electrode in contact with air-saturated 0.10 M HCl. Potential scan rate 50 mV s^{-1}.

If repeated anodic LSVs are performed, the signal A_{Au} decreases progressively whereas the A_{Ag} process increases in height and a second signal ca. 0.80 V (A_*) appears. As can be seen in Fig. 1b for sample Z03, the intensity of the peak A_{Ag} increases notably from the first to the second scan, further increasing slowly or even remaining almost constant. These features can be interpreted by considering: i) that the dissolved silver may remain near the surface and form a UPD layer increasing its effective concentration, and ii) the general phenomenon of desilvering affecting gold objects (vide infra). Accordingly, there will be an Ag concentration gradient in the gold laminas; as the oxidative dissolution of gold advances, more deeper layers of the gold laminas (see again Fig. 2a and b) will be exposed to the electrolyte and the A_{Ag}/C_{Ag} signals increase in successive scans tending apparently to a limiting value.

The signal $A_{Au*}(2)$ can be attributed to the oxidation of active gold sites associated to coordinatively unsaturated surface atoms [27,[30], [31], [32], [33], [34], [35], [36]] whose proportion is enhanced in the second scan as a result of the successive oxidative dissolution-reductive deposition-oxidative dissolution processes occurring during the sequence of the applied voltammetric runs [8]. In turn, the enhancement of the Ag stripping from the first to the second scan can be interpreted as a consequence of the generalized desilvering of gold. In the first scan the intensity of the peak A_{Ag} (1) is representative of the surface concentration of Ag, while ideally, the limiting value of the peak current after several scans will be representative bulk concentration of Ag in the metal with some contribution of the Ag redeposited in the first cathodic scan from the silver ions released in the precedent anodic scans. For simplicity, the intensity of the signal A_{Ag} (2) will be taken as roughly representative of the Ag content in the object.

3.2. Peak current analysis and site characterization

The homogeneity of the voltammetric responses recorded for archaeological gold samples is illustrated by LSVs in Figs. S2 and S3 (Supplementary information). A detailed analysis of the voltammetric curves reveals subtle but consistent differences in the profile of the signals A_{Au} (1). As can be seen in Fig. 2c and d, where the first anodic LSVs recorded on samples SL03 and b) SL05 are depicted, these two samples, both coming from the Santa Llúcia archaeological site, display clearly different peak potentials and peak profiles. This is in contrast with samples from the Mapungubwe site, which display an essentially identical voltammetric response. Given the common archaeological origin of each one of these sets of samples, both found buried at the same site, the most plausible hypothesis is that the differences between samples from the Santa Llúcia site can be attributed to differences in the microcrystalline shape and size distribution, surface roughness, etc. in turn resulting from the differences in the composition and manufacturing technique applied to the piece, as observed for copper/bronze coins (see Refs. [18,22,23] and references herein).

It is pertinent to note that the presence of impurities can distort the observed voltammetric response. Our experimental data, however (see Fig. 1, Fig. 2, Fig. 3, Fig. 4, S1 to S3), consist of homogeneous responses where no additional signals due to trace metals nor electroactive organic compounds (humic materials, for instance) are detected and no differences were detected by comparing archaeological samples with ‘clean’ microcrystalline gold surfaces (samples Z02, Z03). In this context, although different peak potentials have been reported for single crystal gold electrodes with different electrochemically accessible planes ((111) (110), etc.), [25,26,35,39], their influence in the case of microcrystalline, ‘non-clean’ archaeological gold is probably negligible.

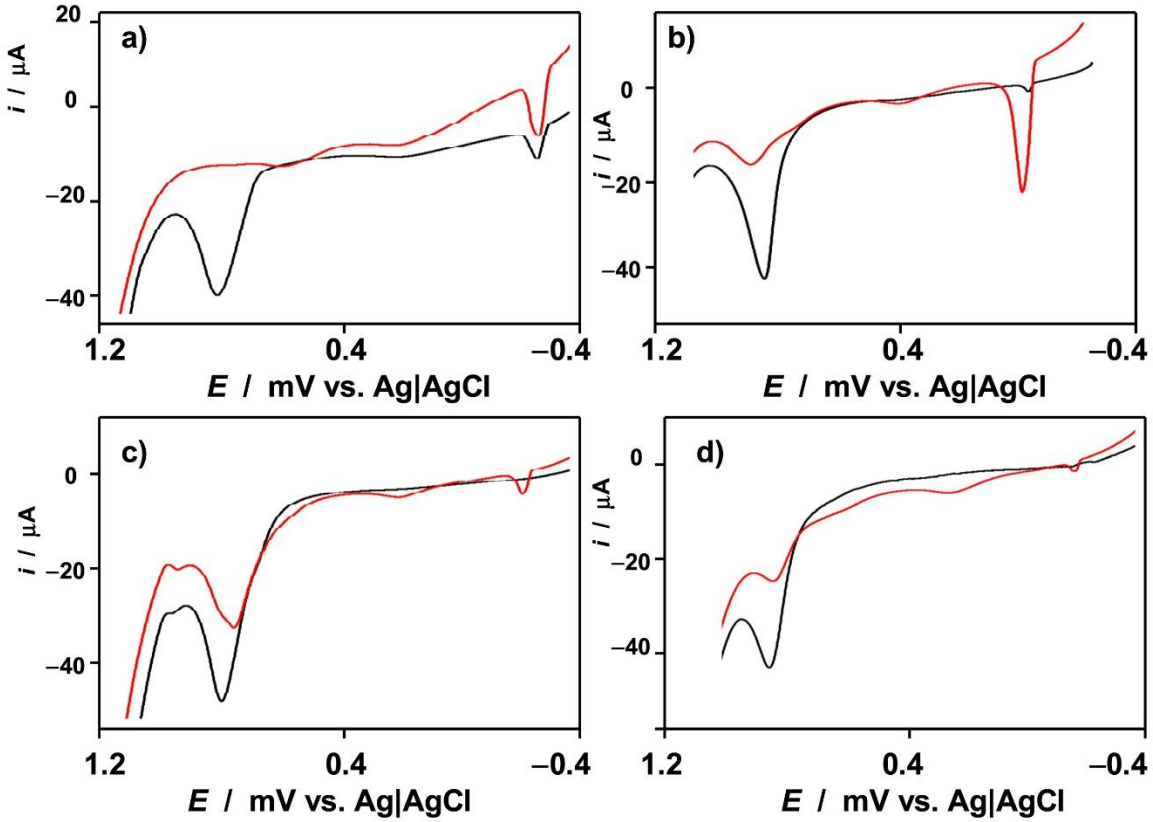

Fig. 3. First (black line) and second (red line) anodic LSVs of samples a) MA03 (dated back to 1300-1400 BCE); b) MA07 ('pilonquitos' dated back to 900-1300 BCE); c) SL05 (dated back to 575 BCE); d) MA01 (unknown age) attached to graphite electrode in contact with air-saturated 0.10 M HCl. Potential scan rate 50 mV s^{-1}.

The above features imply that any attempt to date gold objects has necessarily to compensate the differences in composition and manufacturing processes. The existence of a voltammetric response dependent on age and manufacturing technique is illustrated in Fig. 3 where the voltammograms of samples MA03 (dated back to 1300-1400 BCE); b) MA07 ('pilonquitos' dated back to 900-1300 BCE); c) SL05 (dated back to 575 BCE); d) MA01 (unknown age) are depicted. Here, one can see the existence of significant differences between the position and relative height (i.e. the ratio between the respective peak currents) of the peaks, in particular of peaks A_{Au} (1), A_{Au} (2), A_{Ag} (2). The variations in the position and the profile of the peak A_{Au} (1) can be seen in Fig. 4, where the voltammograms of samples a) Z03; b) MA01; c) MA05; d) MA06, are depicted. The voltammograms of MA05 a necklace dated back to (650 BCE), and MA06, a 'modern' piece added to the same exhibit different profiles in turn differing from those of sample Z03, a ring fabricated in 1988 and the problem sample MA01.

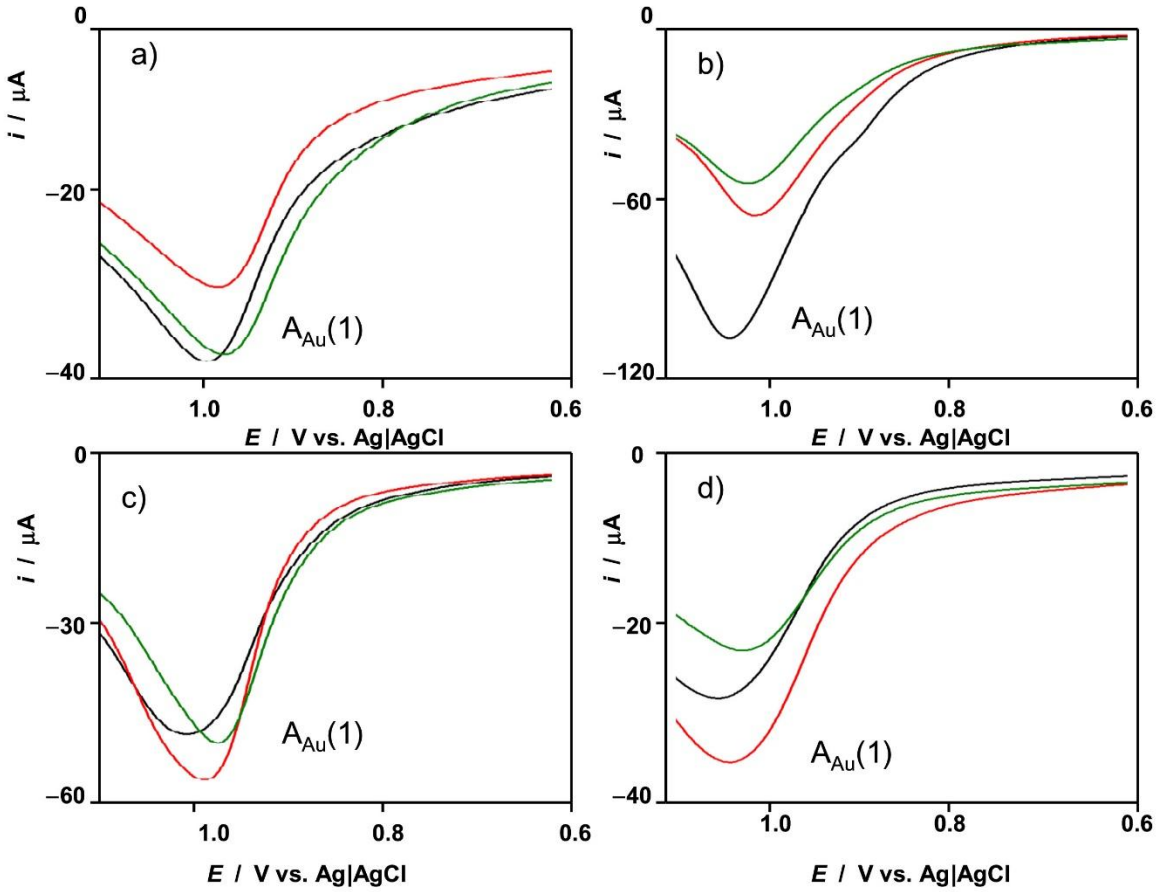

Fig. 4. Detail of the signal A_{Au} (1) recorded in the first anodic LSVs of the following samples: a) Z03; b) MA01; c) MA05; d) MA06, attached to graphite electrode in contact with air-saturated 0.10 M HCl. Potential scan rate 50 mV s^{-1}. Three replicate measurements of each gold sample are superimposed.

One aspect to be taken into account, however, is the possible influence of the total composition of the archaeological metal as well as its deterioration. The presence of silver, which acts as a sacrificial element during corrosion, can be influential on the ageing of gold [43]. In order to account for this possible effect, we tested the variability of the ratio between the peak currents for the oxidation processes A_{Ag} (2) and A_{Au} (1), i_{Ag} (2)/i_{Au} (1). It should be noted that, as far as the net amount of gold sample transferred onto the graphite surface cannot be accurately controlled, only peak current ratios can be used for quantification purposes. The peak currents were measured relative to the base lines depicted in Fig. 1a. These were taken without background subtraction because the scratching of the graphite surface during sampling on gold objects results in a 'true' background current differing from that recorded at the unmodified graphite electrode.

Peak current data reveal significant differences between the different studied samples. The i_{Ag} (2)/i_{Au} (1) ratio can be taken, in principle, as representative of the bulk Ag/Au composition because, as previously noted, the desilvering process implies that the intensity of the peak A_{Ag} (1) does not reflect the bulk Ag proportion in the metal alloy. Interestingly, the samples from the same provenance can be grouped considering simultaneously the i_{Ag} (2)/i_{Au} (1) ratio and the ratio between the sum of the intensities i_{Au} (2) and i_{Au*}(2) and i_{Au} (1).

The corresponding two-dimensional diagram for selected sets of the studied samples is represented in Fig. 5. Remarkably, the Ag content is particularly low in all Mapungubwe samples and in sample MA01. This is a particularly interesting sample of unknown origin and age which will be studied in detail (vide infra). The opposite case is constituted by samples MA07 (three gold bullets, 'pilonquitos', dated back to 900-1300 BCE), presenting high Ag contents.

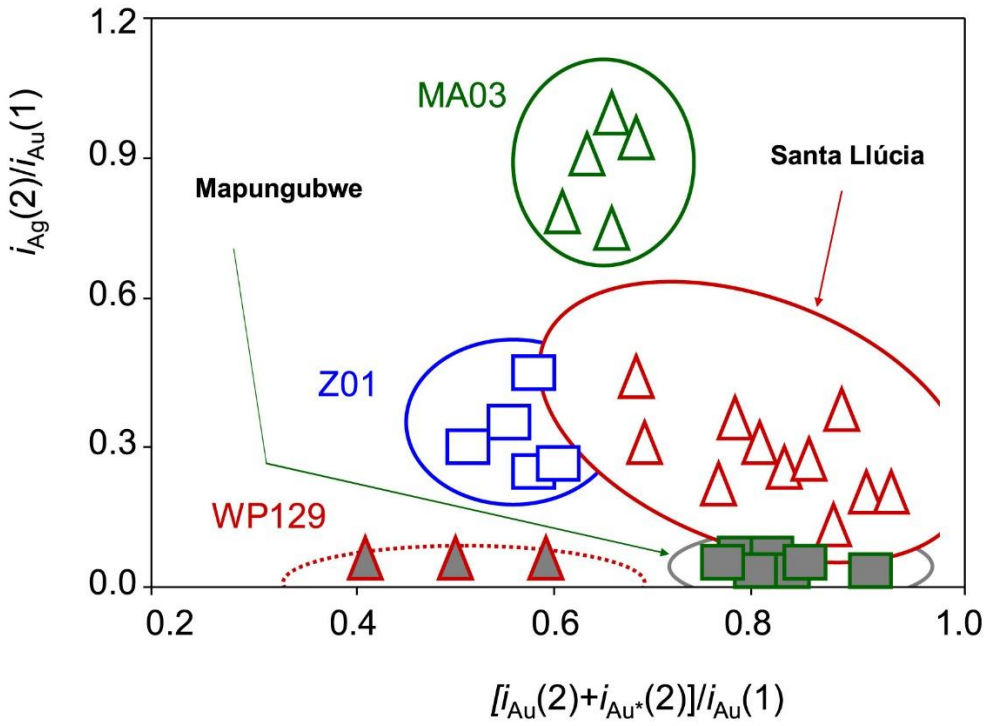

Fig. 5. Two-dimensional diagram containing the ratios [i_{Au} (2) + i_{Au*}(2)]/i_{Au} (1) and i_{Ag} (2)/i_{Au} (1) for several individual gold samples and the samples from Mapungubwe and Santa Llúcia sites.

Noticeably, the voltammetric response of both the Mapungubwe and Santa Llúcia sets of samples produced homogeneous responses when the intensity of the gold-localized peaks A_{Au} (1), A_{Au} (2) and A_{Au*}(2) are considered. This can be seen in Fig. 6, where i_{Au*}(2) is plotted vs. i_{Au} (2). Although with relatively high dispersion –derived mainly from differences in manufacturing– the data points of the 'young' samples Z01-Z03 (from objects dated in the 20th century) can be grouped around a tendency curve (see Fig. 6a) separated from all samples. In turn, the data points of samples from the Mapungubwe gold collection, corresponding to a common origin and a narrow period of time, define a different well-defined curve (Fig. 6b). Consistently, the Santa Llúcia samples, also of the same provenance and attributed to a narrow period of time, fall within a different tendency curve (Fig. 6c) that, as in the precedent cases, can be fitted to a potential function (continuous lines in Fig. 6).

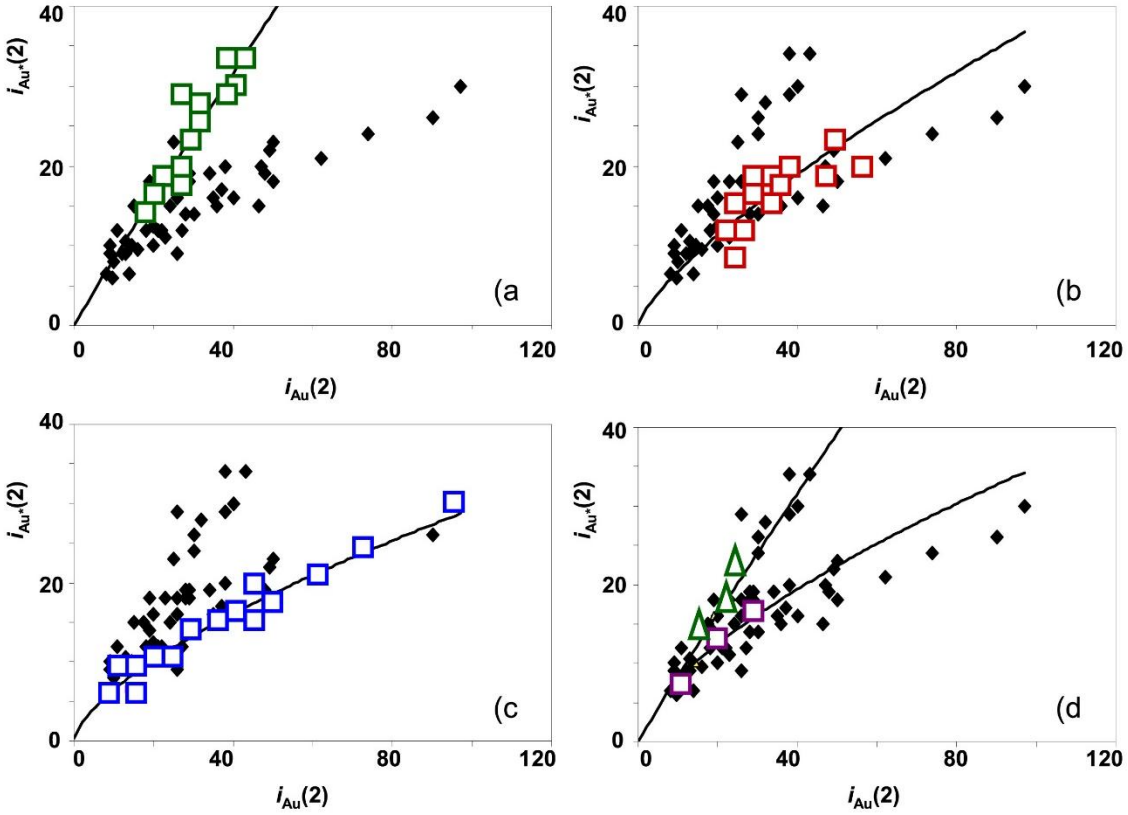

Fig. 6. Plots of the peak current of the process $A_{Au*}(2)$ vs. the peak current for the signal A_{Au} (2) corresponding to gold samples in this study taken from voltammetric data such as in Fig. 1, Fig. 2, underlining different sub-sets of data. a) squares: 'modern' samples Z01-Z03; b) squares: Mapungubwe samples; c) squares: Santa Llúcia samples; d) squares: sample MA01; triangles: sample MA08. The continuous lines correspond to the fit of data points represented by squares to a potential curve.

Two individual samples of particular interest are underlined in Fig. 6d. Sample MA08 corresponds to a recognized modern falsification of an ancient object whereas sample MA01 corresponds to a ring of unknown age with suspect of forgery. In the case of sample MA08, the data points (triangles in Fig. 6d) clearly fall within the tendency graph defined by modern samples consistently with its recognized character of forgery. The data points of sample MA01 (squares in Fig. 6d), however, defined a tendency curve differing from the 'modern' curve. This feature and the extremely low Ag content (see Fig. 5) of this sample suggest that it can be considered as genuinely 'old' from the electrochemical point of view.

Similar grouping of gold samples was obtained using plots of the sum i_{Au} (2) + $i_{Au*}(2)$ vs. i_{Au} (1). This can be seen in Fig. 7 for samples: a) of objects dated in the 20th century, b) Mapungubwe (1200–1290 CE) samples, and c) Santa Llúcia (600-550 BCE) samples. In spite of relatively large dispersion, each set of samples appears to define tendency lines whose slopes increase with the age of the objects. To interpret the grouping of experimental peak current data around tendency lines it has to be taken into account that in the described VIMP experiments it is not possible to control the net amount of metal sample transferred in each sampling onto the graphite surface. Then, the depth reached during the sampling process and hence, the composition of the external gold region varies from one replicate measurement to another.

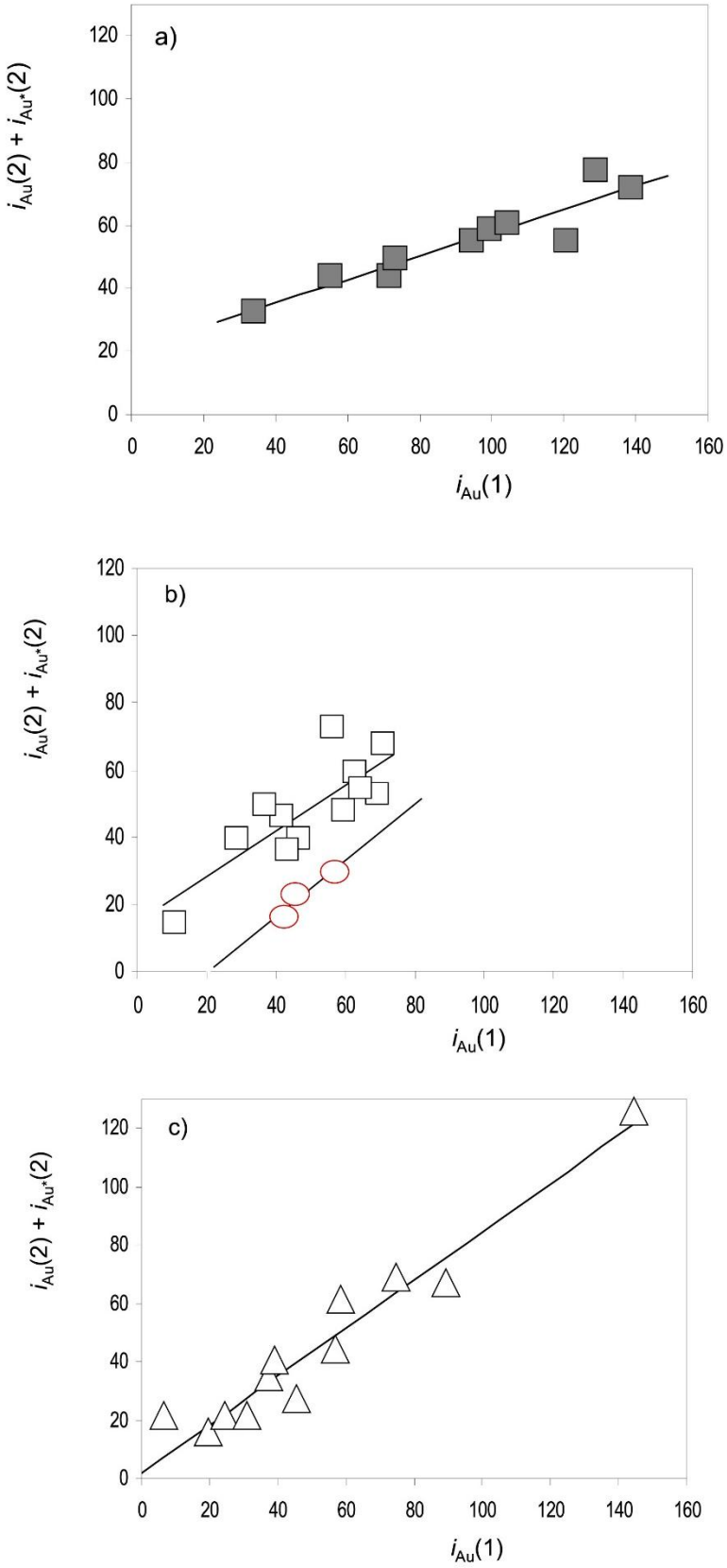

Fig. 7. Variation of the sum of the peak currents for the signals A_{Au} (2) and $A_{Au^*}(2)$, i_{Au} (2) + $i_{Au^*}(2)$ with the peak current for the process A_{Au} (1), i_{Au} (1), for selected sets of samples in this study taken in voltammetric data such as in Fig. 1 a) Samples Z01-Z03 of the 20th century; b) Mapungubwe (1200–1290 CE) samples (squares) and sample MA01 (circles); c) Santa Llúcia (575 BCE) samples.

3.3. Surface analysis

Voltammetric data suggest that there are oxygen species in the surface of gold objects which are distributed following a given in depth pattern. In order to test this view, gold surfaces were examined by means of FIB-FESEM and HRFESM-EDX techniques. Fig. 8a shows the secondary electron image of the obverse of a religious medal dated back from 1902 (sample Z02) in the area in which was performed the trench by fast ion bombardment. Porosity characteristic of the delicate work of goldsmithing was avoided and a polished area was selected as shown in Fig. 8b. Fig. 8c depicts a general view of the trench of (5 × 5) μm. The dimensions selected in the present work accomplish the requirements of quasi-non invasive method for analysis of art and archaeological objects and enable the study of the surface and subsurface of the object that fall within the range of only a few hundred of nm. The image shows the Pt protective coating (marked by an arrow in Fig. 8c) and the granular micromorphology of the Au–Ag–Cu alloy used in the medal and some connected porosity with a clear elongated shape almost parallel to the surface. That was probably due to the stress at which the blank was subjected during the goldsmith work for decorating the field of the medal.

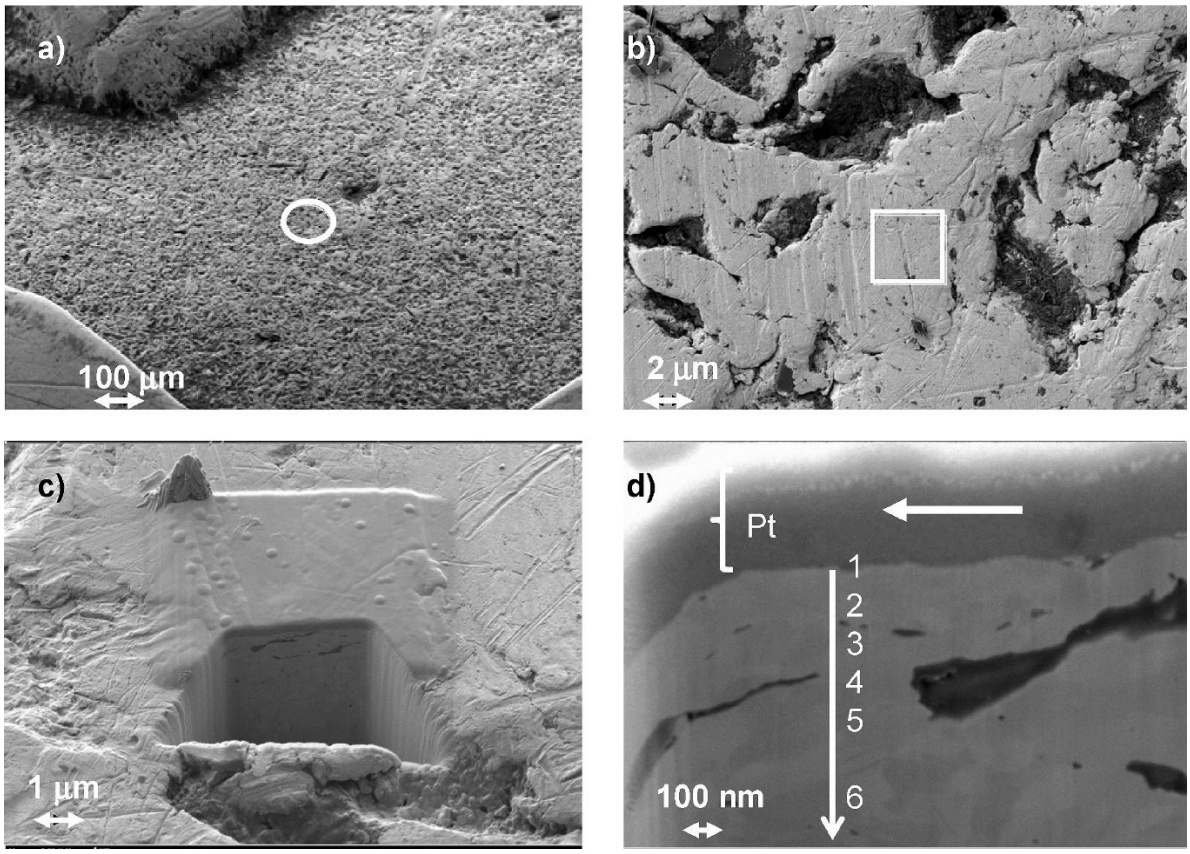

Fig. 8. a) Secondary electron image of the obverse of a religious medal dated back from 1902 in the area in which was performed the trench; b) polished area selected for performing the trench; c) general view of the trench of (5 × 5 μm) with the Pt protecting layer; d) spots for obtaining the X-ray spectra that perform the elemental deep profiling in the surface and sub-surface of the medal.

For performing the elemental deep profiling using the X-ray microanalysis in the surface and sub-surface of the medal a zone exempt of porosity was selected as shown in detail in Fig. 8d. Six X-ray spectra were acquired in spot mode at different deepness and the weight %

oxygen/alloy ratio was calculated from the data provided by the X-ray microanalysis system of the HRFESM which are graphically shown in Fig. 9 (inset).

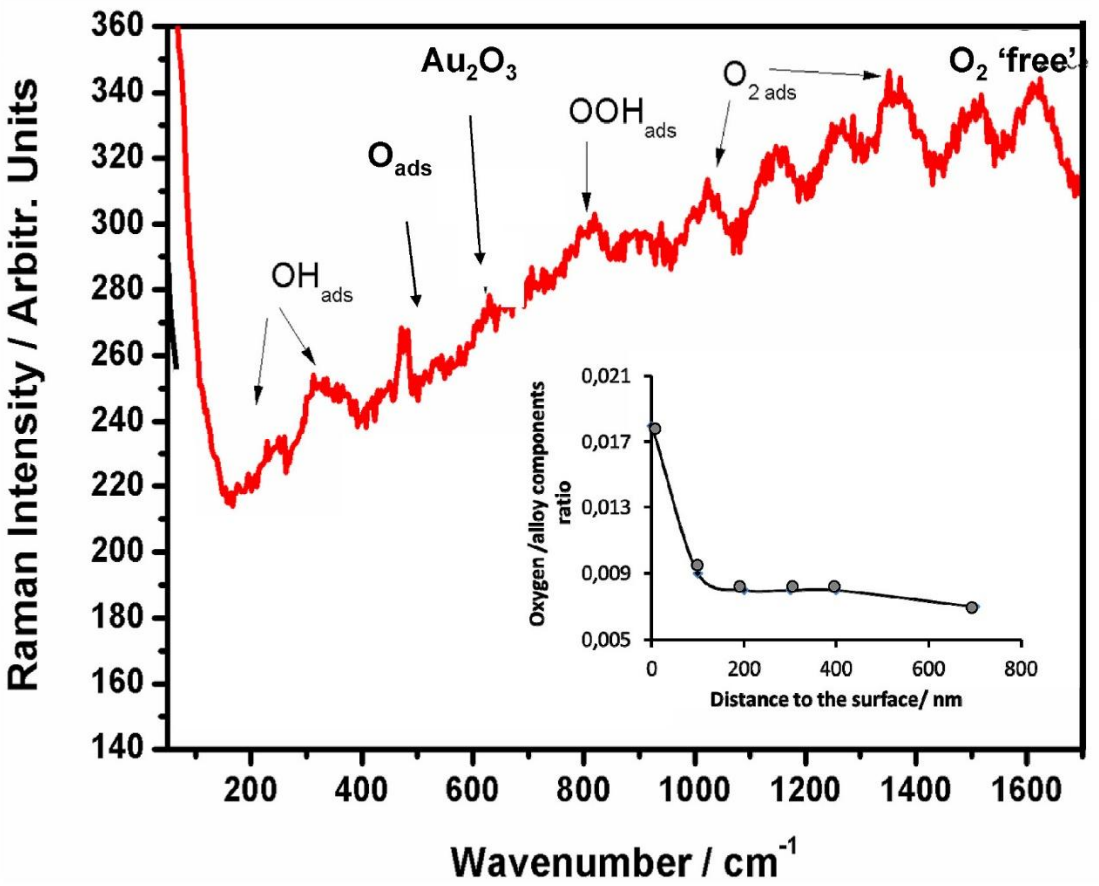

Fig. 9. Raman spectrum of a gold medal dated to 1902. Exposure time 15 s, 40 acquisitions and laser power 60 mW. Inset: Variation of the oxygen/gold mass ratio determined in the trench in Fig. 6d by HRFESM-EDX with depth.

Raman spectroscopy data reveals the variation with depth of the relative abundance of the different oxygen species, in particular, the Raman signatures at 361 cm^{-1} and 449 cm^{-1} associated to ·O adsorbed on Au (111) and Au (211) faces, O–O band at 800 cm^{-1}corresponding to·OOH and O_2 band at 1000 cm^{-1} and the bands at 650 and 635 cm^{-1}, characterizing $Au(OH)_3$ and Au_2O_3 [[44], [45], [46]]. These spectral signatures can be seen in Fig. 9, corresponding to sample Z02. Raman measurements at different depths using a *x*,*y*,*z*-motorized stage, revealed that the intensity of the bands associated to adsorbed ·O, OH, OOH and O_2 tends to decrease with depth whereas the bands of $Au(OH)_3$ and Au_2O_3 increase [8]. Consistently with the assumption that oxygen species are confined to a narrow region in the surface/subsurface region of gold objects, the oxygen/gold mass ratio determined by HRFESM-EDX decreased sharply in the first 100 nm from the surface of the medal (see inset in Fig. 9). Although Raman and HRFESM-EDX data were only accessible for samples Z02 and Z03, their main results, presence of oxygen species adsorbed onto gold surfaces and sharp oxygen concentration gradients in the external gold layer, respectively, can be reasonably assumed to apply for all samples in view of the homogeneous voltammetric response recorded for archaeological samples.

These considerations are also consistent with the variation of the Ag/Au molar ratio (proportional to the i_{Ag} (2)/i_{Au} (1) ratio) with the depth, represented by the absolute value of i_{Au} (1). A comparison of data for the Mapungubwe and Santa Llúcia samples is depicted in Fig. S4 of Supplementary information. One can see that the Santa Llúcia samples exhibit a relatively large variability in the average Ag/Au ratio whereas for the Mapungubwe samples, this ratio is confined to a narrow range between 0.05 and 0.12, consistent with analytical data denoting that Mapungubwe gold samples exhibit a high gold purity with the silver content ranging between 2% and 12% [40,41]. It is important to acknowledge that the silver trace element content is not always the result of intentional alloying, but is considered a contaminant element present (confirmed by energy dispersive X-Ray or EDS) in the Mapungubwe gold material since a relatively higher silver content occurs naturally in South African gold deposits [47]. In southern African archaeological contexts, the result of contamination could be from the melting process, recycling or mixing gold from various sources as reported in comparison with other sites as statistical sampling of gold artefacts differ from natural gold signatures as the Mapungubwe gold samples have elevated Pt concentrations than the natural samples [48]. In contrast, there was no local production of gold in Santa Llúcia and these samples presented higher silver contents with relatively high variability.

Although our voltammetric data characterise Au and Ag responses, it is possible to conjecture that other minority components can influence the aging process. On first examination, this influence can be assumed to be in general low because the 'noble' character of Au results in the preferential oxidation of silver, copper, etc. in the environment forming soluble products which can be released. This gives rise to the well-known phenomenon of the desilvering affecting archaeological objects [49,50] which results in the depletion of the content of Ag (and other oxidizable minority components) in the surface of gold objects.

3.4. Tafel analysis

For dating purposes, the described analysis has the problem that the results are subject to the manufacturing process, leading to relatively high data dispersion. In order to get a better age-dependent response, we have chosen a different approach, i.e., the Tafel analysis of voltammetric curves. The term Tafel analysis is used here in its wide meaning as a method to derive kinetic parameters of an electrochemical process using the linear log$i$ vs. E representations in voltammetric curves (and no necessarily under steady-state conditions). For this purpose, the electrochemical oxidation of gold that proceeds simply through the process described by Eq. (1) is considered. Assuming for simplicity that a unique prevailing complex of stoichiometry $AuCl^{(3-x)-}$ is formed and introducing the equilibrium constant β_x for the complexation process: $Au^{3+}_{(aq)} + xCl^-_{(aq)} \rightarrow AuCl^{(3-x)-}_{(aq)}$, the corresponding Nernst equation can be written as:

$$E^{\circ\prime}{}_{Au} = E^{\circ}\left(Au^{3+}/Au\right) + \frac{RT}{3F}\ln\frac{a_{AuCl_x}}{a_{Au}\beta_x a_{Cl^-}^x} \qquad (2)$$

For a 'clean' gold surface, $a_{Au} = 1$, but for an aged surface it is reasonable to expect that $a_{Au} < 1$ and the formal electrode potential, $E^{\circ\prime}$Au{O} will vary. Assuming that the ageing of gold is mainly due to the formation of O-adsorbates, a highly simplified possibility would be to take $a_{Au\{O\}} \approx 1 - a_{ox}$, a_{ox} being the effective activity of oxygen adsorbates. Then, Eq. (2) leads to:

$$E^{\circ\prime}_{\mathrm{Au\{O\}}} - E^{\circ\prime}_{\mathrm{Au}} = -\frac{RT}{3F}\ln\left(1 - a_{\mathrm{ox}}\right) \tag{3}$$

This means that the gold ageing, in principle, is represented by the increase of a_{ox} with time. As far as this quantity can be assumed to increase monotonically with age, under fixed electrochemical conditions, the variation of $E^{\circ\prime}_{Au\{O\}}$ (or, equivalently, the difference $E^{\circ\prime}_{Au\{O\}} - E^{\circ\prime}_{Au}$) with the aging time can be used for dating gold objects. Assuming that the surface of gold incorporates oxygen adsorbates (O·, HO·, etc.) so that the surface coverage increases monotonically with age (at this stage we neglect oxygen spillover phenomena), and adopting the Lagergren equation for adsorption, consisting of a first-order rate law [8], one can write $a_{\mathrm{ox}} \approx H - Q\mathrm{e}^{-kt}$, where k represents the rate constant for the first-order adsorption kinetics and H, Q are two constant, adjustable parameters. Combining this expression with Eq. (7) one obtains:

$$H - Q\mathrm{e}^{-kt} = 1 - \exp\left[-\frac{3F}{RT}\left(E^{\circ}_{\mathrm{Au\{O\}}} - E^{\circ}_{\mathrm{Au}}\right)\right] \tag{4}$$

equation which relates the ageing time with the variation of the equilibrium potential for the chloride-assisted gold oxidation.

The determination of these formal potentials, however, is made difficult by the fact that the electrochemical process described by Eq. (1) cannot be considered as reversible under our experimental conditions. One first approach could be the use of the Laviron equation that reflects the variation of the peak potential (E_p) with potential scan rate (v) [51]:

$$E_{\mathrm{p}} = E^{\circ\prime} + \frac{RT}{\alpha nF}\ln\left(\frac{k^{\circ}RT}{\alpha nF}\right) + \frac{RT}{\alpha nF}\ln\, v \tag{5}$$

where $E^{\circ\prime}$ represents the formal electrode potential, α the electron transfer coefficient, k° the electrochemical rate constant, A the electrode surface area, and the other symbols have their usual meaning.

The application of this equation implies the performance of voltammograms at different potential scan rates on sample-modified electrodes. Since, even using the minimally invasive VIMP protocol the study of archaeological objects requires to take a limited number of samples, we adopted a different approach based on the Tafel analysis of the voltammetric curve at a given potential scan rate. The expression for the current at an applied potential E is [52]:

$$i = nAFk^{\circ}\Gamma_{\mathrm{o}}\, \exp\left(-\frac{\alpha nF(E-E^{\circ\prime})}{RT}\right) \exp\left[\frac{RTk^{\circ}}{\alpha nFv}\exp\left(-\frac{\alpha nF(E-E^{\circ\prime})}{RT}\right)\right] \tag{6}$$

Here, Γ_o represents the surface area (mol cm^{-2}) of the electroactive species assumed to be uniformly distributed onto the electrode surface. This is not exactly the situation in our case, where micrometer-sized gold laminas adhere to the surface of the graphite electrode (see Fig. 2). Under these circumstances, the peak current can be described by:

$$i_{\mathrm{p}} \approx C\frac{n^2\alpha AF^2\Gamma_{\mathrm{o}}v}{RT} \tag{7}$$

where *C* is a numerical coefficient associated to the shape and size distribution of the gold plates on the graphite surface.

At the initial portion of the voltammetric wave (Tafel region), one can use as a simplified form of Eq. (6):

$$i \approx nAFk^{\circ}\Gamma_{o}\ \exp\left(-\frac{\alpha nF(E-E^{\circ\prime})}{RT}\right) \tag{8}$$

Then, combining Eqs. (7), (8) one obtains:

$$\ln\left(\frac{i}{i_p}\right) \approx \ln\left(\frac{k^{\circ}RT}{Cn\alpha AFv}\right) + \frac{\alpha nF}{RT}E^{\circ\prime} - \frac{\alpha nF}{RT}E \tag{9}$$

Equation that predicts a linear dependence of ln(i/i_p) on *E*, whose slope *s* equals to $-\alpha nF/RT$. The ordinate at the origin *r* will be:

$$r \approx \ln\left(\frac{k^{\circ}RT}{Cn\alpha AFv}\right) + \frac{\alpha nF}{RT}E^{\circ\prime} \tag{10}$$

Then, the formal electrode potential equals to the abscissa at the origin (= *r*/*s*) minus a correction factor: i.e.:

$$E^{\circ\prime} \approx \frac{r}{s} - \frac{RT}{\alpha nF}\ln\left(\frac{k^{\circ}RT}{Cn\alpha AFv}\right) = \frac{r}{s} - \frac{RT}{\alpha nF}\ln\left(\frac{k^{\circ}}{CAv}\right) - \frac{RT}{\alpha nF}\ln\left(\frac{RT}{\alpha nF}\right) \tag{11}$$

The relevant result is that, assuming that there are no large differences in the value of ($RT/\alpha nF$)ln ($k°RT/Cn\alpha AFv$) of the different samples, a calibration graph can be constructed simply by taking the characteristic formal potentials, E_{ccp}, defined from the Tafel plots of ln(i/i_p) vs. *E*, as:

$$E_{ccp} = \frac{r}{s} - \frac{1}{s}\ln s \tag{12}$$

In all cases, Tafel plots of ln(i/i_p) vs. *E* produced representations with satisfactory linearity in terms of correlation coefficients (see Fig. S5 of Supplementary information). Representative data are provided in Table S1 of Supplementary information.

3.5. Calibration graphs

Data in Fig. 7 suggest that the slope of the i_{Au} (2) + i_{Au*}(2) vs. i_{Au} (1) linear representations increase with age (0.37 ± 0.05 for samples Z01-Z03, 0.68 ± 0.16 for Mapungubwe samples, 0.83 ± 0.07 for Santa Llúcia samples). The problem for age calibration purposes is the relatively large dispersion in the values of the peak currents, thus requiring the disposal of a set of samples from the same site for obtaining a reasonable slope in the representation.

Fig. 10a shows the calibration graph obtained for the characteristic potentials E_{ccp} based in the previous Tafel analysis. To some extent surprisingly, this representations tends to show potentials increasing monotonically with the age further slowly decreasing at ages above 1500 years, approximately. A similar qualitative variation was obtained in the representations

of peak potentials (E_p) for the peak A_{Au} (1) vs. age, provided as Fig. S6 in Supplementary information. Interestingly, the dispersion in the values of E_{ccp} is lower than the dispersion of the values of E_p, thus denoting that the Tafel correction compensates significantly the reversibility deviations.

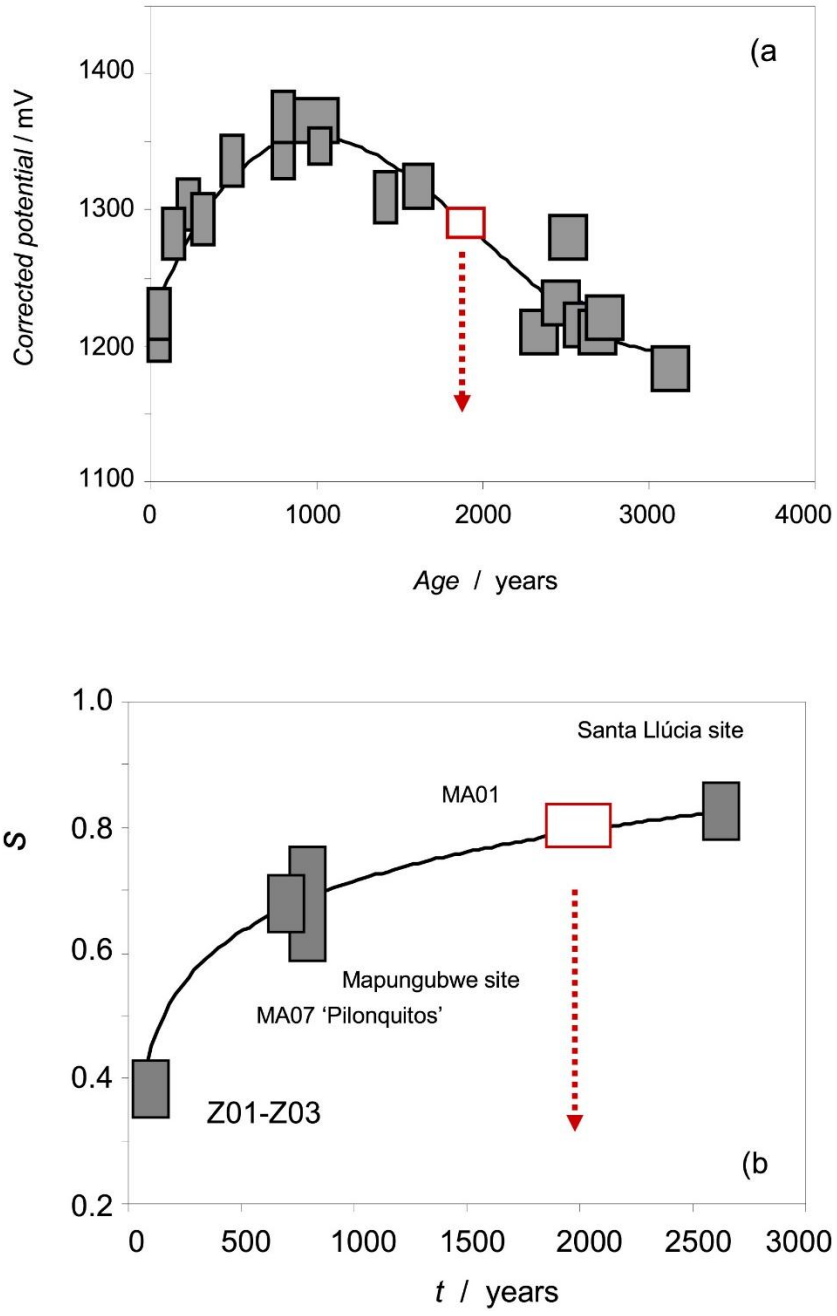

Fig. 10. a) Calibration graph based on the potential E_{ccp} calculated applying Tafel analysis of voltammetric data such as in Fig. 1. The continuous line represents the theoretical curve inserting B = 0.41, k_a = 0.0012 years^{-1} and k_b = 0.0021 years^{-1} into Eq. (16). b) calibration graph based on the slope (s) of the linear dependencies [i_{Au} (2)+i_{Au*}(2)] vs. i_{Au} (1) (cf. Fig. 7). This graph was constructed by fitting the data for samples for which more than 3 data points were available: 'modern' samples Z01-Z03, 'Pilonquitos' (MA07), Mapungubwe samples and Santa Llúcia samples. Solid squares: experimental data used for constructing the calibration curves; squares: data points for the problem sample MA01. The arrows mark the age estimated for this sample using the corresponding calibration graphs.

The peculiar profile of the calibration graphs based on potential measurements can tentatively be interpreted on assuming that a slow spillover phenomenon consisting of the diffusion of O-adsorbed species within the subsurface gold layers can operate. This would follow a scheme proposed to interpret the formation of electrochemically active gold sites via place exchange [27,31,32,34] and catalytic and oxygen interfacial transfer effects on metal oxides deposited on gold electrodes [53,54], and is consistent with the aforementioned data from Raman spectroscopy [8,[44], [45], [46]] and electron microscopy denoting the existence of different O-adsorbates and a gradient of O concentration in the external layers of gold objects. Although there are various superimposed processes associated to the adsorption of different oxygen species in different surface sites, their subsequent diffusion/interchange into subsurface regions, we can adopt a simplified scheme representing the gold aging associated to oxygen functionalities in terms of two successive reactions:

$$Au_{surf} + \{O\} \overset{K_a}{\rightarrow} Au\{O\}_{surf} \overset{K_b}{\rightarrow} Au\{O\}_{sub} \tag{13}$$

where k_a, k_b denote the respective rate constants. On first examination, the activity of Au can be evaluated in terms of the degree of O coverage of the surface as the ratio between the actual surface density of O species, Γ and the maximum attainable surface density of such species, Γ_o. Under conditions of first-order kinetics, the effective activity of Au could be described by an equation of the type:

$$a_{ox} = \frac{\Gamma}{\Gamma_o}\left(e^{-k_a t} - e^{-k_b t}\right) \tag{14}$$

This equation predicts that the effective surface coverage of O adsorbates will diminish with time (age) after reaching a certain minimum level. Combining Eq. (14) with Eq. (3), we obtain

$$E^{\circ\prime}_{Au\{O\}} - E^{\circ\prime}_{Au} = -\frac{RT}{\alpha n F}\left[1 - \frac{\Gamma}{\Gamma_o}\left(e^{-k_a t} - e^{-k_b t}\right)\right] \tag{15}$$

or, equivalently:

$$e^{-k_a t} - e^{-k_b t} = B\left[1 - e^{-\frac{\alpha n F}{RT}\left(E^{\circ\prime}_{Au\{O\}} - E^{\circ\prime}_{Au}\right)}\right] \tag{16}$$

where B is an adjustable parameter. This simplified model agrees well with experimental data so that the age variation of E_{ccp} values in Fig. 10a can be satisfactorily reproduced from Eq. (16) taking $\alpha n = 0.50$ (the usual value for non-reversible electron transfer processes), $B = 0.41$, $k_a = 0.0012$ years^{-1} and $k_b = 0.0021$ years^{-1}.

In Fig. 10b, a second calibration graph, based on the representation of the slope (s) of the linear dependencies of i_{Au} (2) + i_{Au^*}(2) vs. i_{Au} (1) (cf. Fig. 7) vs. time, is depicted. Since the determination of s requires a reasonable number of data points, this representation is restricted to sets of 'modern' samples Z01-Z03, the three 'Pilonquitos' (MA07, three sampling spots for each one) and the Mapungubwe (MU01 to MU06) and Santa Llúcia (SL01-to SL05) collections. This second calibration graph can in principle be rationalized on the basis of the previous kinetic model. Since the i_{Au^*}(2) current is representative of the generation of active defect sites, it should be proportional to the sum of those associated to adsorbed oxygen and those generated by their subsequent diffusion/interchange; i.e.:

$$i^{*}_{\mathrm{Au}}\left(2\right) = 1 - \frac{\Gamma}{\Gamma_{\mathrm{o}}}\left(\mathrm{e}^{-k_a t} + \mathrm{e}^{-k_b t}\right)\right) \tag{17}$$

thus suggesting a continuous growth of i_{Au} (2) + i_{Au^*}(2) on i_{Au} (1).

Inserting the data from three replicate measurements for the problem sample MA01: E_{ccp} = 1303 ± 16 mV, and s = 0.81 ± 0.17, one obtains a common age of 1900 ± 100 years using both calibration graphs in Fig. 10, thus denoting that this problem sample was genuinely of archaeological origin, and entirely consistent with the attribution of this sample made by the archaeologists to a period between 30 BCE and 150 BCE.

4. Conclusions

The proposed new nano-invasive method for electrochemical dating of archaeological gold is based on the age dependence of the equilibrium potential of gold oxidative dissolution in HCl electrolytes. That dissolution is affected by oxygen species adsorbed on the metal surface, and it is quantified relative to the 'clean' gold surface. Applying a correction for irreversibility based on the Tafel analysis of the voltammetric curve, the obtained equilibrium potentials vary monotonically with the age for a series of gold samples coming from different museums and collections. In particular, this methodology yields a satisfactory dating for samples of the archaeological sites of Mapungubwe Gold Collection, dated back to 1200–1290 CE and the collection from the Santa Llúcia, Alcalà de Xivert (Spain) dated back 600-550 BCE and different samples from the Mannheim Museum covering a time span of ca. 3500 years. The most remarkable result is that samples could be satisfactorily dated, which not only come from different continents, but the ages of which cover more than 3000 years. This clearly highlights that the storage conditions are of surprisingly little effect, of course, provided that the surface has not been polished or treated otherwise in a destructive way. It is also noteworthy that the sampling has been performed by different local scientists, which clearly shows the robustness of this dating approach.

CRediT authorship contribution statement

Antonio Doménech-Carbó: Conceptualization, Methodology, Funding acquisition, Formal analysis, Writing - original draft, Writing - review & editing. **Fritz Scholz:** Data curation, Formal analysis, Writing - original draft, Writing - review & editing. **Michael Brauns:** Data curation, Formal analysis, Writing - original draft, Writing - review & editing. **Sian Tiley-Nel:** Data curation, Formal analysis, Writing - review & editing. **Arturo Oliver:** Data curation, Formal analysis, Writing - review & editing. **Gustavo Aguilella:** Data curation, Formal analysis, Writing - review & editing. **Noemí Montoya:** Data curation, Formal analysis, Writing - review & editing. **María Teresa Doménech-Carbó:** Data curation, Formal analysis, Writing - original draft, Writing - review & editing.

Declaration of competing interest

The authors declare no conflicto of interest.

Acknowledgements

Project CTQ2017-85317-C2-1-P, supported with Ministerio de Economía, Industria y Competitividad (MINECO), Fondo Europeo de Desarrollo Regional (ERDF) and Agencia Estatal de Investigación (AEI), is gratefully acknowledged. The authors wish to thank Mr. Manuel Planes, Dr. José Luis Moya and Mrs. Alicia Nuez Inbernón, technical supervisors of the Electron Microscopy Service of the Universitat Politècnica de València and Arno Braun for organizing the ring from Hermeskeil and the trust of the responsible leadership of the Rhenische Landesmuseum Trier, Dr. Marcus Reuter and the Universität des Saarlandes, Prof. Dr. Sabine Hornung. In addition, Maggi Loubser for her valued critique and peer comments on the chemistry and analytical content and Sandra Markgraaf for assistance with the preparation of the graphite bars for the South African samples on the Mapungubwe gold Collection from the University of Pretoria Museums.

References

[1] M.J. Aitken, Science-Based Dating in Archaeology, Longman, New York, 1990(chapter 8).

[2] G. Artioli, Scientific Methods and Cultural Heritage, Oxford Univ. Pres., 2010.

[3] S. Reich, G. Leitus, S. Shalev, Measurement of corrosion content of archaeological lead artifacts by their Meissner response in the superconducting state; a new dating method, New J. Phys.5 (2003) 99, 199.9.

[4] O. Eugster, Dating gold artifacts applications for noble gas analysis of gold,Gold Bull. 29 (1996) 101-104.

[5] O. Eugster, J. Kramers, U. Krähenbühl, Detecting forgeries among ancient gold objects using the U, Th-4He dating method, Archaeometry 51 (2009) 672-681.

[6] A. Doménech-Carbó, M.T. Doménech-Carbó, M.A. Peiró-Ronda, Dating archaeological lead artifacts from measurement of the corrosion content using the voltammetry of microparticles, Anal. Chem. 83 (2011) 5639-5644.

[7] A. Doménech-Carbó, M.T. Doménech-Carbó, S. Capelo, T. Pasíes-Oviedo,I. Martínez-Lázaro, Dating archaeological copper/bronze artifacts using the voltammetry of microparticles, Angew. Chem. Int. Ed. 53 (2014) 9262-9266.

[8] A. Doménech-Carbó, F. Scholz, M.T. Doménech-Carbó, J. Piquero-Cilla,N. Montoya, T. Pasíes-Oviedo, M. Gozalbes, J.M. Melchor-Montserrat, A. Oliver, Dating of archaeological gold by means of solid state electrochemistry, ChemElectroChem 5 (2018) 2113-2217.

[9] F. Scholz, B. Meyer, in: A.J. Bard, I. Rubinstein (Eds.), Voltammetry of Solid Microparticles Immobilized on Electrode Surfaces, Electroanalytical Chemistry, A Series of Advances, vol. 20, Marcel Dekker, New York, 1998, pp. 1-86.

[10] F. Scholz, U. Schröder, R. Gulabowski, A. Doménech-Carbó, Electrochemistry of Immobilized Particles and Droplets, second ed., Springer, Berlin-Heidelberg,2014.

[11] A. Doménech-Carbó, J. Labuda, F. Scholz, Electroanalytical chemistry for the analysis of solids: characterization and classification (IUPAC Technical Report), Pure Appl. Chem. 85 (2013) 609-631.

[12] D. Blum, W. Leyffer, R. Holze, Pencil-Leads as new electrodes for abrasive stripping voltammetry, Electroanalysis 8 (1996) 296-297.

[13] E. Ottenwelter, V. Costa, Evidence of metallic plating on archaeological artefacts by voltammetry of microparticles, Archaeometry 57 (2015) 497-504.

[14] A. Doménech-Carbó, M.T. Doménech-Carbó, V. Costa, in: F. Scholz (Ed.), Electrochemical Methods in Archaeometry, Conservation and Restoration(Monographs in Electrochemistry Series, Springer, Berlin-Heidelberg, 2009.

[15] A. Doménech-Carbó, M.T. Doménech-Carbó, Electroanalytical techniques in archaeological and art conservation, Pure Appl. Chem.90 (2018) 447-462,2018.

[16] F. Scholz, U. Schröder, S. Meyer, KhZ. Brainina, N.F. Zakharchuk, N.V. Sobolev,O.A. Kozmenko, The electrochemical response of radiation defects of non-conducting materials an electrochemical access to age determinations, J. Electroanal. Chem. 385 (1995) 139-142.

[17] A. Doménech-Carbó, M.T. Doménech-Carbó, J. Redondo-Marugán, L. Osete-Cortina, J. Barrio, A. Fuentes, M.V. Vivancos-Ramón, W. Al-Sekhaneh,B. Martínez, I. Martínez-Lázaro, T. Pasíes-Oviedo, Electrochemical characterization and dating of archeological leaded bronze objects using the voltammetry of immobilized particles, Archaeometry 60 (2018) 308-324.

[18] F. Di Turo, N. Montoya, J. Piquero-Cilla, C. De Vito, F. Coletti, G. Favero, M.T. Doménech-Carbó, A. Doménech-Carbó, Dating archaeological strata in the *magna mater* temple using solid-state voltammetric analysis of leaded bronze coins, Electroanalysis 30 (2018) 361-370.

[19] X. Ferragud, J. Piquero-Cilla, M.T. Doménech-Carbó, V. Guerola-Blay,X. Company, A. Doménech-Carbó, Electrochemical analysis of gildings in Valencia Altarpieces: a cross-age study since 15th until 20th century, J. Solid State Electrochem. 21 (2017) 1477-1487.

[20] B. Martínez, J. Piquero-Cilla, N. Montoya, M.T. Doménech-Carbó, A. Doménech-Carbó, Electrochemical analysis of gold embroidery threads from archaeological textiles, J. Sólid State Electrochem.22 (2018) 2205-2215.

[21] A. Doménech-Carbó, Dating - an analytical task-, ChemTexts 1 (2015) 5.

[22] A. Doménech-Carbó, A, Electrochemical dating: a review, J. Solid State Elec-trochem.21 (2017) 1987-1998.

[23] A. Doménech-Carbó, F. Scholz, Electrochemical age determinations of metallic specimens - the utilization of the corrosion clock, Acc. Chem. Res. 52 (2019)400-406.

[24] J. Herrera-Gallego, C.E. Castellano, A. Calandra, A.J. Arvia, The electrochemistry of gold in acid aqueous solutions containing chloride ions, J. Electroanal.Chem. 66 (1975) 207-230.

[25] D.M. Kolb, J. Schneider, Surface reconstruction in electrochemistry: gold (100)-(520), gold (111)-(123), and gold (110)-(12), Electrochim. Acta 31(1986) 929-936.

[26] H. Angerstein-Kozlowska, B.E. Conway, A. Hamelin, L. Stoicoviciu, Elementary steps of electrochemical oxidation of single-crystal planes of Au-I, Chemical basis of processes involving geometry of anions and the electrode surfaces, Electrochim. Acta 31 (1986) 1051-1061.

[27] L.D. Burke, A.P. O'Mullane, Generation of active surface states of gold and the role of such states in electrocatalysis, J. Solid State Electrochem. 4 (2000)285-297.

[28] M. Tian, W.G. Pell, B.E. Conway, Nanogravimetry study of the initial stages of anodic surface oxide film growth in HClO4and H2SO4by means of EQCM, Electrochim, Acta 48 (2003) 2675-2689.

[29] P.S. Germain, W.G. Pell, B.E. Conway, Evaluation and origins of the difference between double-layer capacitance behaviour at Au-metal and oxidized Ausurfaces, Electrochim. Acta 49 (2004) 1775-1788.

[30] F. Scholz, G. Lopez de Lara-Gonzalez, L.M. de Carvalho, L. Hilgemann,KhZ. Brainina, H. Kahlert, R.S. Jack, D.T. Minh, Indirect electrochemical sensing of radicals and radical scavengers in biological matrices, Angew. Chem. Int. Ed.46 (2007) 8079-8081.

[31] A. Nowicka, U. Hasse, G. Sievers, M. Donten, Z. Stojek, S. Fletcher, F. Scholz, Selective knockout of gold active sites, Angew. Chem. Int. Ed. 49 (2010) 3006.[

32] S. Cherevko, N. Kulyk, C.-H. Chung, Utilization of surface active sites on gold in preparation of highly reactive interfaces for alcohols electrooxidation in alkaline media, Electrochim. Acta 69 (2012) 190-196.

[33] U. Hasse, K. Fricke, D. Dias, G. Sievers, H. Wulff, F. Scholz, Grain boundary corrosion of the surface of annealed thin layers of gold by OH-radicals, J. Solid State Electrochem. 16 (2012) 2383-2389.

[34] S. Cherevko, N. Kulyk, C.-K. Chung, Utilization of surface active sites on gold in preparation of highly reactive interfaces for alcohols electrooxidation in alkaline media, Electrochim. Acta 69 (2012) 190-196.

[35] U. Hasse, H. Wulff, C.A. Helm, F. Scholz, Formation of gold surfaces with a strongly preferred {100}-orientation, J. Solid State Electrochem. 17 (2013)3047-3053.

[36] R.L. Doyle, M.E.G. Lyons, The mechanism of oxygen evolution at super-activated gold electrodes in aqueous alkaline solution, J. Solid State Electro-chem. 18 (2014) 3271-3286.

[37] R.G.P. Giron, G.S. Ferguson, Development of cathodic silence in an oxide film on gold electrode, Electrochim. Acta 180 (2015) 560-563.

[38] O. Kasian, N. Kulyk, A. Mingers, A.R. Zerajdanin, K.J.J. Maryhofer, S. Cherevko, Electrochemical dissolution of gold in presence of chloride and bromide traces studied by on-line electrochemical inductively-coupled plasma mass spectrometry, Electrochim. Acta 222 (2016) 1056-1063.

[39] C. Jeyabharathi, P. Ahrens, U. Hasse, F. Scholz, Identification of low-index crystal planes of polycrystalline gold on the basis of electrochemical oxide layer formation, J. Solid State Electrochem. 20 (2016) 3025-3031.

[40] S. Woodbourne, M. Pienaar, S. Tiley-Nel, The dating of the gold graves from Mapungubwe hill, J. African Archaeol.7 (2009) 95-101.

[41] S. Tiley-Nel, A. Botha, Conservation of the Mapungubwe gold collection, J. Ite.Cons.36 (2013) 65-80.

[42] G. Aguilella, Primeros datos sobre el asentamiento del Hierro Antiguo de Santa Llúcia (Alcalà de Xivert, Castellón). Sector 1, fase 2, Quaderns de Prehistória iArqueologia de Castelló 34 (2016) 105-118.

[43] D.A. Scott, The deterioration of gold alloys and some aspects of their conservation, Stud. Conserv. 28 (1983) 194-203.

[44] O. Diaz-Morales, F. Calle-Vallejo, C. de Munck, M.T.M. Koper, Electrochemical water splitting by gold: evidence for an oxide decomposition mechanism, Chem. Sci. 4 (2013) 2334-2343.

[45] J. Desilvestro, M.J. Weaver, Surface structural changes during oxidation of gold electrodes in aqueous media as detected using surface-enhanced Raman spectroscopy, J. Electroanal. Chem. 209 (1986) 377-386.

[46] B.S. Yeo, S.L. Klaus, P.N. Ross, R.A. Mathies, A.T. Bell, Identification of hydroperoxy species as reaction intermediates in the electrochemical evolution of oxygen on gold, ChemPhysChem 11 (2010) 1854-1857.

[47] N. Desai, N. Technological, Social and Economic Aspects of Gold Production and Use by the Iron Age People of Southern Africa, Doctoral dissertation, University of Cape Town), 2001.

[48] R. Netshitungulwana, An Investigation of the Trace Element Compositions of Gold from Zimbabwe and South Africa: Implications for Tracing the Source of Archeological Gold Artefacts, Doctoral dissertation, University of the FreeState), 2011.

[49] S. Schlosser, A. Reinecke, R. Schwab, E. Pernicka, S. Sonetra, V. Laychour, Early Cambodian gold and silver from Prohear: composition, trace elements and gilding, J. Archaeol. Sci. 39 (2012) 2877-2887.

[50] S. Liu, T. Rehren, J. Chen, C. Xu, P. Venunan, D. Larreina-Garcia, M. Martinón-Torres, Bullion production in imperial China and its significance for sulphide ore smelting world-wide, J. Archaeol. Sci. 55 (2015) 151-165.

[51] E. Laviron, General expression of the linear potential sweep voltammogram in the case of diffusionless electrochemical systems, J. Electroanal. Chem. 101(1979) 19-28.

[52] J.C. Myland, A.M. Bond, Quasireversible cyclic voltammetry of a surface confined redox system: a mathematical treatment, Electrochem. Commun. 7(2005) 282-287.

[53] A.M. Chaparro, Study of spillover effects with the rotating disk electrode, Electrochim. Acta 58 (2011) 691-698.

[54] A. Doménech-Carbó, F. Sabaté, J. Sabater, Electrochemical analysis of catalytic and oxygen interfacial transfer effects on MnO_2 deposited on gold electrodes,J. Phys. Chem. C 122 (2018) 10939-10947.